Prediction of Necking and Fracture Based on the Crystal Plasticity

Jong-Bong Kim[1], Won-Sang Seo[2], Seung-Hyun Hong[3], Jeong Whan Yoon[4]

[1] Dept. of Automotive Engineering., SeoulTech, Korea, jbkim@seoultech.ac.kr; [2] Graduate School of NID Fusion Technol., SeoulTech, Korea; [3] Sheet Metal Development TFT, R&D Division for Hyundai Motor Company and Kia Motors Corporation, Korea; [4] Faculty of Engineering & Industrial Sci., Swinburne Univ. of Technol., Australia

Abstract. In order to predict necking and fracture phenomena, a crystal plasticity model is introduced in the finite element analysis of tensile tests. Grains having different orientations are subjected to numerical tensile tests. A damage model is also proposed to predict the sudden drop of load carrying capacity after necking and to reflect the void nucleation and growth on the severely deformed region. From the analyses of tensile test, the necking and fracture phenomena are well predicted.

Keywords: Fracture, Necking, Crystal plasticity

1. INTRODUCTION

In sheet metal forming processes, necking and fractures need to be accurately predicted in order to make defect free products. A forming limit diagram (FLD) [1-3] is a well-known and powerful measure for fracture prediction. In the ordinary stamping process, the necking strain and the fracture strain are almost the same because deformation after necking takes place in very local regions and averaged strain in a grid can be measured. The FLD obtained with averaged strain in a grid, therefore, can be used in the prediction of fractures in general sheet metal forming processes such as stamping and deep drawing.

In specific sheet metal forming processes such as the incremental forming process, however, local fracture strain is important because the deformation takes place in very local regions. The local deformation is considered to be the main reason of the formability improvement in incremental sheet metal forming. In most tensile tests, elongation, engineering strain, and true strain are measured with a gauge attached on the specimen and the values are averaged. However, the local fracture strain is far greater than the averaged one.

In order to investigate the fracture behaviour after necking, tensile test is subjected to the finite element analysis based on crystal plasticity and damage evolution. Without the evolution of damage, or material softening due to the damage, the sudden drop of load carrying capacity cannot be described [4]. Nielsen and Tvergaard [4] analysed necking and fracture behaviour of friction stir welded sheets using the modified Gurson model [5]. In the ductile fracture model, damage evolution is described by void nucleation, growth and coalescence [6]. Void nucleation, growth and coalescence are modelled by mathematical equations and many coefficients have to be decided in order to use the experimental data.

In this study, it is assumed that voids or cracks are nucleated where stress is concentrated by orientation mismatch. Each grain has its own orientation. Therefore, the orientation of one grain does not coincide with that of its neighbour grains and stress concentration may take place. To analyse the stress concentration inside a grain, crystal plasticity is introduced in the analysis of the tensile test. Crystal plasticity is widely used to predict material behaviour such as anisotropy development, twinning, and crack initiation. Yoon et al. [7] studied the anisotropic hardening behaviour of cube textured aluminium alloy sheets using the crystal plasticity model. Choi et al. [8] analysed the stress concentration on the grain boundary and the twining behaviour of Mg alloys. They used electron backscatter diffraction (EBSD) data to allocate the grain orientation to the regular mesh. Dao and Li [9] predicted crack initiation in bending using the crystal plasticity model. They used the representative volume element (RVE) method to assign the orientation to regular elements. Lin et al. [10] predicted the crack propagation path near the crack tip under cyclic loads.

In this study, the crystal plasticity finite element method is employed to predict necking and fracture behaviour. A damage model is also proposed to describe the sudden drop of tensile load carrying capacity. From the analysis results, it is shown that the proposed damage model based on crystal plasticity describes the fracture behaviour and void nucleation well.

2. THEORY

2.1. Crystal plasticity model

The crystal plasticity model accounts for the deformation of a material by crystallographic slip and for the reorientation of the crystal lattice. In this work, a rate-dependent TBH model, which was well described by Dao and Asaro [11], is employed. The deformation gradient $[F]$ is decomposed into a plastic deformation ($[F^p]$) and a combination of elastic deformation and rigid body motion of the crystal lattice ($[F^e]$), i.e.,

$$[F] = [F^e][F^p]. \tag{1}$$

Equation (1) leads to the decomposition of the deformation rate, $[L]$, into elastic and plastic parts as

$$[L] = [L^e] + [L^p]. \tag{2}$$

Since the plastic deformation is assumed to be due to dislocation slip, the plastic deformation rate $[L^p]$ is determined by the summation of the shear strain contribution over the entire slip system [11], as

$$[L^p] = \sum_{(s)} \dot{\gamma}^{(s)} \{b^{(s)}\} \{n^{(s)}\}. \tag{3}$$

Here, *(s)* means a slip system, and $\{n^{(s)}\}$ and $\{b^{(s)}\}$ are the normal to the slip plane and the vector in the slip direction, respectively. The symmetric ($[D]$) and skew symmetric ($[W]$) parts of the velocity gradient can be written as:

$$[D^p] = \frac{1}{2}\left([L^p] + [L^p]^T\right) = \sum_{(s)} \dot{\gamma}^{(s)} \frac{1}{2}\left(\{b^{(s)}\}\{n^{(s)}\} + \{n^{(s)}\}\{b^{(s)}\}\right), \quad (4a)$$

$$[W^p] = \frac{1}{2}\left([L^p] - [L^p]^T\right) = \sum_{(s)} \dot{\gamma}^{(s)} \frac{1}{2}\left(\{b^{(s)}\}\{n^{(s)}\} - \{n^{(s)}\}\{b^{(s)}\}\right). \quad (4b)$$

The Jaumann rate of the Kirchhoff stress can be expressed in terms of the total deformation rate and the plastic part as

$$[\overset{\nabla}{\tau}] = [K]:([D]-[D^p]) - [W^p]\cdot[\tau] + [\tau]\cdot[W^p], \quad (5)$$

where $[K]$ is a fourth-order tensor based on the anisotropic elastic modulus $[C]$. Incorporating Equations (4a) and (4b) into Equation (5), the Jaumann stress rate becomes

$$[\overset{\nabla}{\tau}] = [K]:[D] - \sum_{(s)} \dot{\gamma}^{(s)}[R_{(s)}], \quad (6)$$

where $[R_{(s)}]$ is a rotation tensor that depends on the slip plane normal and direction. Equation (6) is used to update the stress at the integration point after the unknowns $\dot{\gamma}^{(s)}$ are solved at the slip system level. The determination process of the unknowns $\dot{\gamma}^{(s)}$ is described in detail in the work of Yoon et al. [7].

2.2. Damage model

Wierzbicki et al. [12] intensively reviewed the prediction capability of various damage models. Johnson and Cook [13] defined the critical equivalent fracture strain as a monotonic function of the stress triaxiality. Wierzbicki et al. [12] assumed that fracture occurs when the accumulated equivalent plastic strain, modified by the function of the stress triaxiality and the deviatoric state parameter, reaches the critical value. Cockcroft and Latham [14] proposed a damage model as a function of principal stress and effective strain. In this study, a new damage model is proposed as follows.

$$dD = \begin{cases} \dfrac{\sigma_1 d\varepsilon_1}{\sigma_{cr}\cdot\Delta\varepsilon_{cr}} & for\ \ \sigma_1 \geq \sigma_{cr}\ \ and\ \ d\ \ \varepsilon_1 \geq 0, \\ 0 & for\ \ \sigma_1 < \sigma_{cr}\ \ or\ \ d\ \ \varepsilon_1 < 0 \end{cases}. \quad (7)$$

$$D = \int dD \quad (8)$$

In Equation (7), σ_{cr} is the critical major stress over which damage starts to accumulate and $\Delta\varepsilon_{cr}$ is the plastic strain amount from damage initiation to fracture. In this study, $\Delta\varepsilon_{cr}$ is called the "degradation plastic strain". If the major stress is less than the critical stress, or if the deformation along the major stress is compressive, the damage increment is zero. σ_{cr} and $\Delta\varepsilon_{cr}$ are material parameters that should be determined.

3. ANALYSIS MODEL FOR TENSILE TEST

3.1. Finite element model

To predict necking and fracture phenomena, tensile tests for a 6022-T4 aluminium alloy sheet are subjected to the finite element analysis based on the crystal plasticity model. The crystal plasticity model and the damage model described in the previous chapter are implemented into the finite element code ABAQUS/Explicit [15] via a user-defined material subroutine (VUMAT). For the analysis of the stress concentration due to the orientation mismatch, the element size should be smaller than the grain size and a great number of elements are needed for the whole tensile specimen. For computational effectiveness, therefore, the analysis domain is reduced, as shown in figure 1. Tensile displacements are imposed for the upper and lower faces. For the left face of the selected domain, displacement along the x-direction is set to zero. No boundary condition is imposed on the right face.

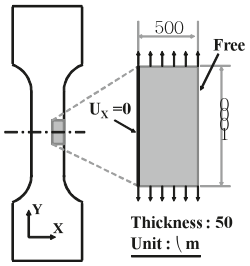

Figure 1. Definition of analysis domain and boundary conditions for tensile test.

Figure 2 shows the grain shapes and element discretization. Grain shape is assumed to be a regular hexagon and grain size is assumed to be about 40 μm. Each grain is discretized by about 45 elements, as shown in figure 2(c), and the same orientation angles are allocated to all elements in each grain. The elements in each grain are sorted in one group and orientations are allocated. Figure 3 shows the contour of '-cos(ϕ)', where ϕ is the second Euler angle. It is shown that the same orientation angles are allocated to all elements in each grain.

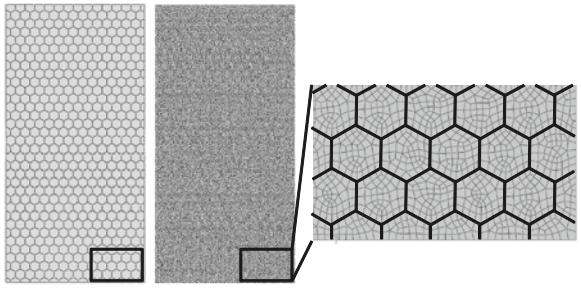

(a) (b) (c)

Figure 2. (a) Grain shapes, (b) element discretization, and (c) detailed view of element shape.

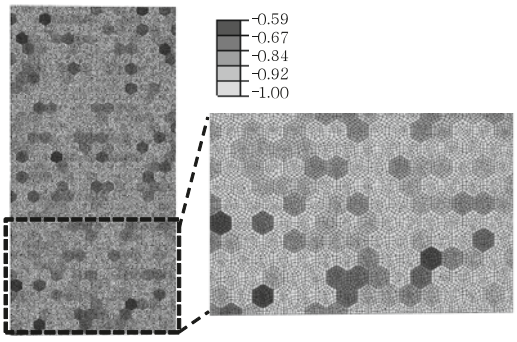

Figure 3. Contour of "-cos(ϕ)" showing the correct allocation of orientation angles.

3.2. Material properties

A 6022-T4 aluminium alloy sheet is used in the analysis. Basic mechanical properties obtained by tensile test along

the transverse direction are shown in table 1. The slip resistance of all slip systems at one material point is taken to be the same. The slip system hardening is assumed to follow the macroscopic hardening behaviour. Through several trial analyses, the average Taylor factor is determined to be 2.253 and the following hardening equation is used for the slip system hardening.

$$\bar{\sigma}_{(s)} = 197.3\ (\varepsilon + 0.002)^{0.257}. \quad (9)$$

Figure 4 shows the analysed stress-strain curve using the slip system hardening of Equation (9). The curve is in good agreement with the measured curve. Figure 5 shows the (111) pole figure for the 6022-T4 aluminium alloy. The pole figure is measured using standard X-ray diffraction techniques and orientation imaging microscopy (OIM).

Table 1. Mechanical properties of 6022-T4 aluminium alloy sheet along the transverse direction.

Uniform elongation	23 %	
Total elongation	28 %	
UTS	295.7 MPa	
Hardening : $\sigma=K(\varepsilon+\varepsilon_0)^n$	K	444.6 MPa
	ε_0	0.002
	n	0.257

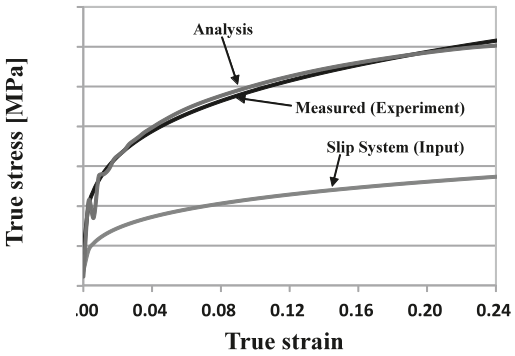

Figure 4. Comparison of stress-strain curves obtained by analysis and experiment.

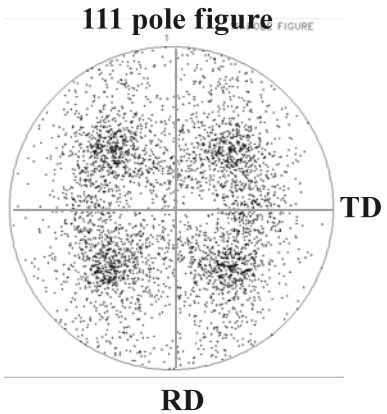

Figure 5. (111) Pole figure for 6022-T4 sheet sample.

4. SIMULATION RESULTS AND DISCUSSION

Figure 6 shows the major stress distributions at several time stages. As expected, stress concentration takes place at many points. This stress concentration is considered to be caused by orientation mismatches between neighbour grains. As tensile strain increases, the stress concentration also becomes bigger until the stress reaches the critical value. If the major stress becomes greater than this critical value, damage starts to accumulate and stress is lowered by softening. In figure 6, it is interesting that the local major stress in some regions is far greater than the fracture stress measured by tensile tests. This means that the local stress can be far greater than the averaged global stress.

Figure 7 shows the evolution of damage in the case of σ_{cr}=500 MPa and $\Delta\varepsilon_{cr}$=0.1. When the global true strain is 0.145 (Figure 7(c)), the damage value starts to accumulate at many points. This can be correlated with the concept of void nucleation. When the global strain is 0.210 (Figure 7(d)), the damage values starts to accumulate at more points and the damaged area increases. This is similar to void growth. When the global tensile strain is 0.241 (figure 7(e)), some damaged regions get together and this is similar to void coalescence. Figure 7(f) shows that fracture takes place on the slant, as usual for a ductile material. As a result, figure 7 shows the void nucleation, growth and coalescence process very well.

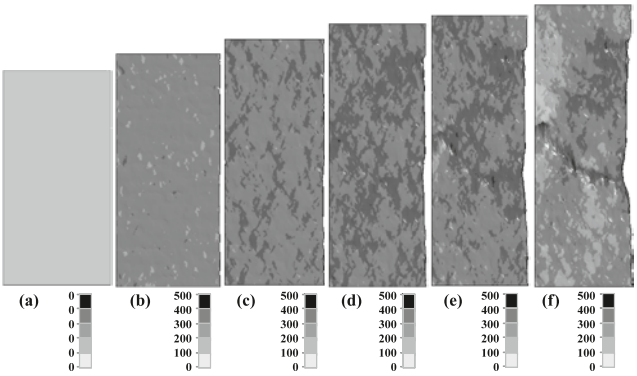

Figure 6. Major stress distributions when (a) $\varepsilon_{1,g}$=0.000, (b) $\varepsilon_{1,g}$=0.075, (c) $\varepsilon_{1,g}$=0.145, (d) $\varepsilon_{1,g}$=0.210, (e) $\varepsilon_{1,g}$=0.241 and (f) $\varepsilon_{1,g}$=0.272.

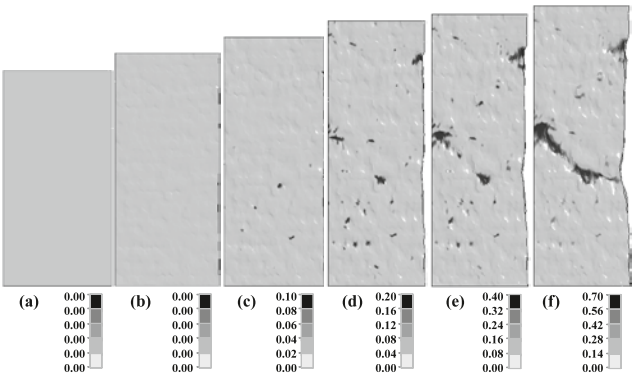

Figure 7. Damage value distributions when (a) $\varepsilon_{1,g}$=0.000, (b) $\varepsilon_{1,g}$=0.075, (c) $\varepsilon_{1,g}$=0.145, (d) $\varepsilon_{1,g}$=0.210, (e) $\varepsilon_{1,g}$=0.241 and (f) $\varepsilon_{1,g}$=0.272.

In order to investigate the effect of the critical stress and the degradation plastic strain on the damage evolution, the deformed shapes and the damage distributions are shown in figure 8. In the case of low critical stress (figures 8 (a) and (b)), two narrow fracture bands are formed in the early stage of the tensile test; these bands are almost perpendicular. As the critical stress increases, the localized

deformation band becomes wider. In the case of figures 8 (c)~(e), only one fracture band is shown. The degradation plastic strain value has not much effect on the fracture band width and direction. However, the degradation plastic strain has an effect on the strain localization speed.

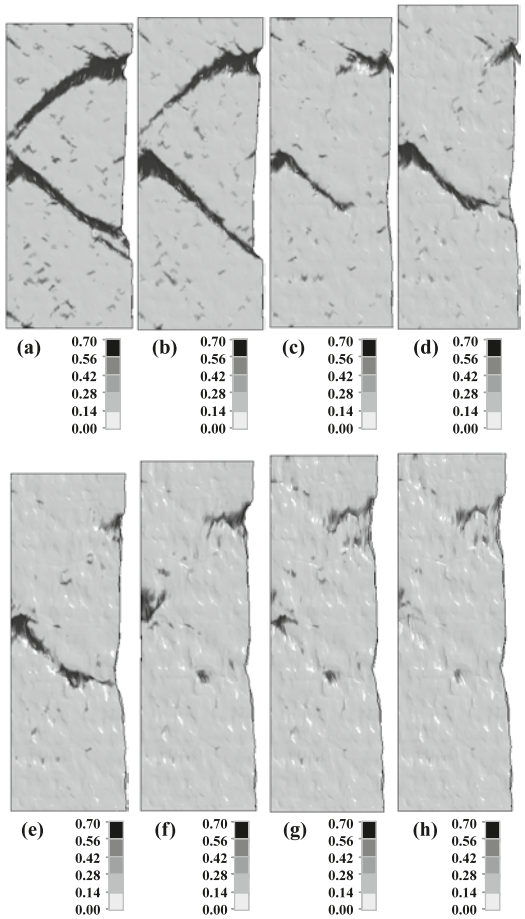

Figure 8. Damage value distributions for various values of the critical stress and the degradation plastic strain: (a) σ_{cr}=300, $\Delta\varepsilon_{cr}$ =0.1 ($\varepsilon_{1,g}$=0.145); (b) σ_{cr}=300, $\Delta\varepsilon_{cr}$ =0.3 ($\varepsilon_{1,g}$=0.162); (c) σ_{cr}=400, $\Delta\varepsilon_{cr}$ =0.1 ($\varepsilon_{1,g}$=0.162); (d) σ_{cr}=400, $\Delta\varepsilon_{cr}$ =0.3 ($\varepsilon_{1,g}$=0.210); (e) σ_{cr}=500, $\Delta\varepsilon_{cr}$ =0.1 ($\varepsilon_{1,g}$=0.272); (f) σ_{cr}=500, $\Delta\varepsilon_{cr}$ =0.3 ($\varepsilon_{1,g}$=0.301); (g) σ_{cr}=550, $\Delta\varepsilon_{cr}$ =0.1 ($\varepsilon_{1,g}$=0.329); (h) σ_{cr}=550, $\Delta\varepsilon_{cr}$ =0.3 ($\varepsilon_{1,g}$=0.329).

Table 2. Predicted uniform elongation and total elongation.

σ_{cr}	Uniform elongation (%)		Total elongation (%)	
	$\Delta\varepsilon_{cr}$ =0.1	$\Delta\varepsilon_{cr}$ =0.3	$\Delta\varepsilon_{cr}$ =0.1	$\Delta\varepsilon_{cr}$ =0.3
300 MPa	6	8	8	10
400 MPa	12	16	14	19
500 MPa	22	25	25	28
550 MPa	27	27	30	30

Uniform and total elongations predicted by the finite element analyses are shown in table 2. From a comparison of the data in table 2 with the experimental data shown in table 1, the critical stress and degradation plastic strain are determined to be 500 MPa and 0.1, respectively.

5. CONCLUSIONS

The necking and fracture behaviours of 6022-T4 aluminium sheet are analysed based on a crystal plasticity model. To describe the sudden drop of load carrying capacity after necking, a damage model is proposed. Stress concentration is observed at many points due to the orientation mismatch at the grain boundary; this stress concentration causes damage initiation and evolution. The void nucleation, growth and coalescence phenomena are well described by the proposed methodology. Finally, the necking and fracture behaviours are also well predicted. With this methodology, it is shown that micro-cracks during forming can also be predicted

6. REFERENCES

[1] S.B. Kim, H. Huh, H.H. Bok, M.B. Moon: Forming limit diagram of auto-body steel sheets for high-speed sheet metal forming, J. of Mater. Process. Technol., 211 (2010), 851-862.
[2] M. Kuroda, V. Tvergaard: Forming limit diagrams for anisotropic metal sheet with different yield criteria, Int. J. of Solids and Struct., 37 (2000), 5037-5059.
[3] T.B. Stoughton, J.W. Yoon; A new approach for failure criterion for sheet metals, Int. J. Plasticity, 27 (2011), 440-459.
[4] K.L. Kielsen, V. Tvergaard; Effect of a shear modified Gurson model on damage development in a FSW tensile specimen, Int. J. Solids and Struct., 46 (2009), 587-601.
[5] V. Tvergaard, A. Needleman; Analysis of the cup-cone fracture in a round tensile bar, Acta Mater., 32 (1984), 157-169.
[6] Z.L. Zhang, C. Thaulow, J. Odegard; A complete Gurson model approach for ductile fracture, Engineering Fracture Mech., 67 (2000), 155-168.
[7] J.W. Yoon, F. Barlat, J.J. Gracio, E. Rauch; Anisotropic strain hardening behaviour in simple shear for cube textured aluminium alloy sheets, Int. J. Plasticity, 21 (2005), 2426-2447.
[8] S.-H. Chio, D.H. Kim, S.S. Park, B.S. You; Simulation of stress concentration in Mg alloys using the crystal plasticity finite element method, Acta mater., 58 (2010), 320-329.
[9] M. Dao, M. Li; A micromechanical study on strain-localization-induced fracture initiation in bending using crystal plasticity models, Philosophical Magazine A, 81 (2001), 1997-2020.
[10] B. Lin, L.G. Zhao, J.Tong; A crystal plasticity study of cyclic constitutive behaviour, crack-tip deformation and crack-growth path for a polycrystalline nickel-based superalloy, Engineering Fracture Mech., 78 (2011), 2174-2192.
[11] M. Dao, R.J. Asaro; Localized deformation modes and non-schmid effects in crystalline solids. Part I. Crytical conditions of localization, Mech. Mater., 23 (1996), 71-102.
[12] T. Wierzbicki, Y. Bao, Y.-W. Lee, Y. Bai; Calibration and evaluation of seven fracture models, Int. J. Mech. Sci., 47 (2005), 719-743.
[13] G.R. Johnson, W.H. Cook; Fracture characteristics of three metals subjected to various strain, strain rate, temperatures and pressures, Eng. Fract. Mech., 21 (1985), 31-48.
[14] M.G. Cockcroft, D.J. Latham; Ductility and the workability of metals; J. of the Institute of Metals, 96 (1968), 33-39.
[15] ABAQUS theory manual, version 6.4, 2006, ABAQUS Inc.

Acknowledgements. This work was supported by a National Research Foundation of Korea Grant funded by the Korean Government (NRF-2011-013-D00001), and the Korea Institute for Advancement of Technology (KIAT) through the Workforce Development Program in Strategic Technology.

